Available online at www.sciencedirect.com
ScienceDirect
Journal of Hazardous Materials 152 (2008) 765–777
Journal of Hazardous Materials
www.elsevier.com/locate/jhazmat

Reactive dyes remotion by porous TiO_2-chitosan materials

Carolina E. Zubieta, Paula V. Messina*, Carina Luengo, Mariana Dennehy, Olga Pieroni, Pablo C. Schulz

Departamento de Química, Universidad Nacional del Sur, 8000 Bahía Blanca, Argentina

Received 18 March 2007; received in revised form 16 July 2007; accepted 16 July 2007
Available online 20 July 2007

Abstract

In this work, the aim was to evaluate the remotion (adsorption plus degradation) of two reactive dyes, Methylene Blue (MB) and Benzopurpurin (BP), from aqueous solutions by the utilization of TiO_2-chitosan microporous materials.

Two different TiO_2-chitosan hybrid materials were synthesized: TiO_2-Chit A with 280 mg chitosan/gTiO_2 and TiO_2-Chit B with 46.76 mg chitosan/g TiO_2. Adsorption data obtained at different solution temperatures (25, 35, and 45 °C) revealed an irreversible adsorption that decrease with the increment of *T*. Langmuir, Freundlich and Sips isotherm equation were applied to the experimental data. The obtained parameters and correlation coefficient showed that the adsorption of both dyes on TiO_2-Chit A at the three work temperatures was best predicted by the Langmuir isotherm, while Sips equation adjusted better to adsorption data on TiO_2-Chit B.

The adsorption enthalpy was relatively high and varied with *T*, indicating that interaction between adsorbent and adsorbate molecules was not only physical but chemical. There is a change in the adsorption heat capacity, ($\Delta_{ads}C_p < 0$), related with intense hydrophobic interactions.

The kinetic adsorption data were processed by the application of Lagergren and Avrami models. It was found that adsorption of both dyes on both adsorbents under the operating conditions was best predicted by Avrami model. The variation of kinetic order, *n*, and k_{av} with *T* are related to a pore followed by intra particle diffusion control of the adsorption rate.

MB photodegradation on both TiO_2-chitosan hybrid materials was of 91 (in A) and 41% (in B) and augmented with the chitosan content. For BP can be seen that the process in darkness resulted in a high remotion capacity than in UV light presence.

Keywords: Chitosan; TiO_2; Dye remotion; Photodegradation

1. Introduction

Reactive dyes are the largest single group of dyes used in the textile industry. Being highly water-soluble, it is estimated that 10–20% of reactive dyes remains in the wastewater during the production process of these dyes [1] and nearly 50% of reactive dyes may be lost to the effluent during dying process of cellulose fibers [2]. Furthermore, it is projected that 10–20% of dyes in the textile sector will be lost in residual liquors through incomplete exhaustion and washing operations. The rate of loss is approximated to be 1–2 and 10% for pigments and leather dyes. Effluent treatment process for dyes are currently able to get rid of about half of the dyes lost in residuals liquors. Therefore, about 400 tonnes daily [3] find their way into the environment, primarily dissolved or suspended in water.

Adsorption is a physicochemical wastewater treatment process, which is gaining prominence as a means of producing high quality effluents, which are low in concentrations of dissolved organics.

The requirements of an adequate adsorptive capacity restrict the choice to microporous adsorbents with pore diameter ranging from a few Angstroms to a few tens of Angstroms. This includes both traditional microporous adsorbents such as activated carbon and the more recently developed crystalline alumino silicates or zeolites. Activated carbon is the most popular used adsorbent in wastewater treatments [4] and it is widely used for the removal of color [5]. However, activated carbon has to be regenerated off sites with losses of about 10% in the thermal regeneration process. Other tested adsorbents, such as eucalyptus bark and clay that are throwaway products, can only be used once and have to be disposed of afterwards [6].

* Corresponding author. Tel.: +54 291 4551447; fax: +54 291 4551447.
E-mail address: pau423ve@yahoo.com.ar (P.V. Messina).

0304-3894/$ – see front matter © 2007 Elsevier B.V. All rights reserved.
doi:10.1016/j.jhazmat.2007.07.043

Semiconductor photocatalysis has attracted a great deal of attention in recent years. The strong oxidative power of photogenerated holes on semiconductor surface has made them a most suitable photocatalytic material in environmental remediation. Photoexitation of semiconductors generates electron-holes pair capable of attracting organic dyes either directly or indirectly by means of highly reactive species during their reaction with the solvent and/or additives [7–9].

In general TiO_2 is recognized as the most efficient, non-toxic, and stable photocatalyst. Mechanistically, the photocatalyst TiO_2 is first exited by UV light and subsequently initiates the photodegradation process.

In this work, the aim was to evaluate the remotion (adsorption plus degradation) of reactive dyes from aqueous solutions by the utilization of TiO_2-chitosan microporous materials. Several reports have recently been devoted to this problem and indicated that such materials are one of the most important of the new advanced oxidation technologies to be applied to water purification [10]. Chitosan is obtained by *N*-deacetylation of chitin, the next most abundant natural polysaccharide after cellulose [11]. It is an invaluable renewable natural resource whose technological importance is becoming increasingly evident. Numerous reports on the applications of chitosan, ranging from wastewater treatment [12] to biomedical and pharmaceutical applications [11] can be found in literature. Chitosan is extremely attractive due to its biocompatibility, biodegradability and no toxicity [11,12] along with its fungistatic and antibacterial activity [12–14]. Recent applications of chitin and chitosan are found, for instance, in studies of the removal of metal ions [15] and dyes [16,17] from aqueous solutions. In aqueous solutions, the amine groups of chitosan are much easier to cationize and they adsorb dye anions strongly by electrostatic attraction. However, pure chitosan has some disadvantages such as unsatisfactory mechanical properties, severe shrinkage, deformation after drying, solubility under acidic conditions, and compressibility at high operating pressure. Several methods to overcome these disadvantages have been performed by coating or impregnating chitosan on rigid porous materials such as silica gel [18].

The cationic polyelectrolyte at the TiO_2 surface incorporation, possibilities the adsorption of both acid and basic dyes. Since the deacetylated amino groups in chitosan can be protonated, the polycationic properties of the polymer can be expected to contribute to the charged interaction with anionic dyes and at the same time decreased the adsorption capacity of TiO_2 material for the basic dye adsorption. To evaluated both last effects and obtain the best material which would provide the major adsorption capacity for both dyes simultaneously, two different TiO_2-chitosan material were synthesized: TiO_2-Chit A with 280 mg chitosan per gram of TiO_2 and TiO_2-Chit B with 46.76 mg chitosan/g TiO_2.

On the other hand, the employ of a photocatalytic TiO_2 adsorbent provides a destructive oxidation process utilizing the more effective, inexpensive and inexhaustive solar energy that reaches the earth surface to treat the dye-containing wastewaters. In such process, there is no consumption of expensive oxidizing chemicals, the oxidant is atmospheric oxygen and the catalyst is non-hazardous.

2. Experimental

2.1. Materials and methods

The TiO_2 material synthesis was performed by a surfactant template route as follows [19]: 11.6 ml of Ti (IV) Isopropoxide (Ti (IV) $(iPrO)_4$) was mixed with 2 ml double distilled water and stirred by 2 min at 500 rpm. Then a solution of 7.65 g of Hexadecyltrimethylammoniun bromide (HTAB, also known as CTAB) in 38 ml water was added to the first one. The resulting gel was stirred by 3 min and left 48 h in hydrothermal treatment at 100 °C in autoclave. The obtained gel was filtered, washed several times with double distilled water and left to dry at room temperature. Then it was calcined by 7 h at 540 °C under air flux.

Chitosan [α(1–4) 2-amino 2-deoxy β-D glucan] was kindly supplied by The Chitin basic and applied research laboratory (LIBAQ) of Universidad Nacional del Sur, Bahía Blanca, Argentina. Chitosan is soluble in weak acids like acetic acid. The pK_a is 6.3. The following characterizations were performed (details not shown), in order to check some important aspects, concerning the purity and structural aspects of the chitosan sample: the degree of deacetylation (75%) was determined by UV spectrophotometry [20]. Solid-state ^1H NMR spectroscopy, XRD and FT-IR were used to verify the purity of chitosan sample. The total quantity of nitrogen (% and mol g^{-1}) was determined by the Kjeldhal method [20,21].

Two reactive dyes, methylene blue (MB, cationic) and benzopurpurin (BP, anionic,) were chosen as adsorbates. MB is a basic blue dyestuff, C.I. classification number 52015, $\lambda_{max} = 661$ nm, $M_w = 373.9$ g mol^{-1}. BP is an anionic dye, C.I. classification number 23,500, Direct Red 2, $\lambda_{max} = 500$ nm, $M_w = 724.73$ g mol^{-1}.

All reagents, including acetic acid, were obtained from Aldrich and were of analytical grade (99%). Both dyes were utilized without further treatment. For aqueous dye solutions only double-distilled water was used. Solution pH was kept constant and equal to 8.0 by the employ of a phosphate (Na_2HPO_4/NaH_2PO_4) buffer.

Two hundred milligrams of the TiO_2 material were kept in contact with 20 mL of different concentrations chitosan acetic solutions, (0.1–2) wt.%, during 48 h with continuous stirring at 500 rpm. Then, the mixture was centrifuged and the supernatant was separated. The solid residue (TiO_2 plus adsorbed chitosan) was filtered to avoid acetic acid excess, drying under vacuum until constant weight and calcined by 7 h at 540 °C under air flux. The amount of chitosan adsorbed is computed by the mass difference between the non-calcined and the calcined material. This procedure was done at three different temperatures (25, 35, 45 °C).

For the dye adsorption and degradation experiments, two chitosan solutions (0.5 and 1 wt.%) were chosen. The TiO_2 material was kept in contact with chitosan (as it was mentioned above), filtered and washed several times with double distilled water to avoid the acetic excess and dry under air flux until constant weight.

The synthesized TiO_2-chitosan material characterization was performed by the techniques usually employed in porous materials.

2.1.1. Nitrogen adsorption isotherms

The nitrogen adsorption isotherms at 77.6 K were measured with a Micrometrics Model Accelerated Surface Area and Porosimetry System (ASAP) 2020 instrument. Each sample was degassed at 373 K for 720 min at a pressure of 10^{-4} Pa.

2.1.2. Transmission electron microscopy

Transmission electron microscopy was performed using a JEOL 100 CX II transmission electron microscope, operated at 100 kV with magnification of 100,000×. Observations were made in a bright field. Powdered samples were placed on cooper supports of 2000 mesh.

2.1.3. FT-IR spectroscopy

FT-IR experiments were recorded in a Nicolet FT-IR Nexus 470 Spectrophotometer. To avoid co-adsorbed water the samples were dried under vacuum until constant weight was achieved and diluted with KBr powder before the FT-IR spectra were recorded.

2.1.4. X-ray powder diffraction

Powder X-ray diffraction (XRD) data were collected via a Philips PW 1710 diffractometer with Cu Kα radiation (λ = 1.5418 Å) and graphite monochromator operated at 45 kV; 30 mA and 25 °C.

The material stability under different pH conditions was evaluated according to the industrial pH effluents (pH 4–10). TiO_2-chitosan material was packed in a chromatographic column and eluted with different pH (4, 6, 8, and 11) solutions (pH was regulated by the addition of the property amounts of HCl and NaOH concentrated solutions (1 M)). The eluted fraction was studied by ATR-FTIR spectroscopy using a ZnSe crystal, to evaluate the presence of desorbed chitosan. Experiments were performed with a Nicolet Magna 560 FTIR equipped with a DTGS detector. Each spectrum is the result of 256 co-added interferograms. The spectral resolution was 2 cm^{-1} in all cases. The working temperature in these experiments was 25 ± 2 °C.

Adsorption experiments (in darkness to avoid photodegradation) were carried out in 5 ml glass-stopped round bottom flasks immersed in a thermostatic shaker bath. For this, 50 mg of adsorbent were mixed with 5 ml of aqueous dye solutions with (0.00834–0.048) mmol/L concentration range. The flasks with their content were shaken at 25, 35 and 45 °C. The stirring speed was kept constant at 90 rpm. At the end of the adsorption period, the supernatant was centrifuged for 1 min at a speed of 3000 min^{-1}. The supernatant MB and BP concentration before and after adsorption was determined using a Spectronic −20 UV–vis spectrophotometer at 664 and 504 nm, respectively.

To study the effect of the photodegradation, the same experiments were carried out in presence of UV light at T = 25 °C. A DESAGA UV 131000 lamp (λ = 366 nm) was applied as a radiation source for the photodegradation of dyes. Light intensity was estimated as $I_a = 2.7 \times 10^{-6}$ mol photon s^{-1} [22]. To discriminate between both effects (adsorption and photodegradation) the results of the experiments without light were subtracted from those carried out under irradiation. The photodegradation effect on dye solutions was confirmed by the application of ATR-FTIR.

Equation fitting were done from non-linear procedures using ORIGIN®computer package (release 7.0).

3. Results and discussion

3.1. Chitosan-TiO_2 material characterization

Fig. 1 shows the chitosan adsorption isotherms on the TiO_2 material. The isotherms show the typical form of type F [23] isotherms indicating an interaction between adsorbate molecules stronger than that between adsorbate and adsorbent. In this case, the uptake of chitosan molecules is initially slow until surface coverage is sufficient so that interactions between adsorbed and free molecules begin to dominate the process. One might say that the process is autocatalytic in terms of the adsorption process [24]. The polyelectrolyte adsorption increased with the increment of T, which is associated with an endothermic process. The heat of adsorption is lower than the heat of condensation [23]. No practical differences could be appreciated from the chitosan adsorption at 35 and 45 °C.

The quantity of adsorbed chitosan on TiO_2 material at the conditions employed in the dye degradation were 280 mg chitosan/g TiO_2 (TiO_2-Chit A) and 46.76 mg chitosan/g TiO_2 (TiO_2-Chit B) for the material in contact with chitosan acetic solution 0.5 and 1 wt.%, respectively. More than 1 wt.% concentrated chitosan solution were too much viscously to work and less than 0.5 wt.% represent a minor chitosan adsorption at the TiO_2 surface.

In consideration to the industrial effluents pH which varies from 4 to 10 in textile industry, the stability of chitosan layers adsorbed on TiO_2 material was studied.

The ATR-FTIR spectrum of elution samples is shown in Fig. 2. As it was in solution, the chitosan characteristic band (due

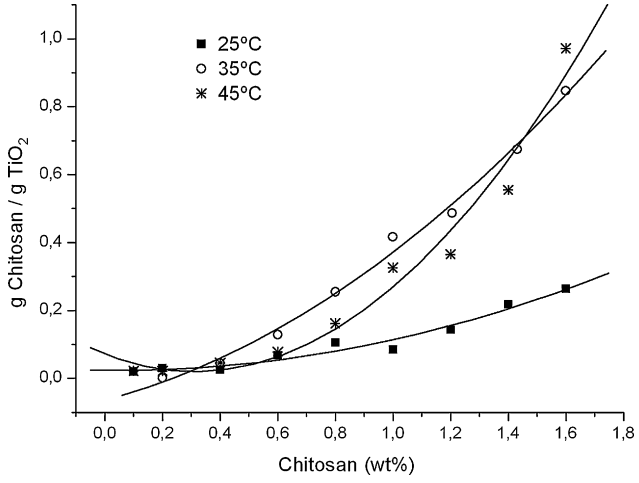

Fig. 1. Chitosan adsorption isotherms on the TiO_2 material at different temperatures.

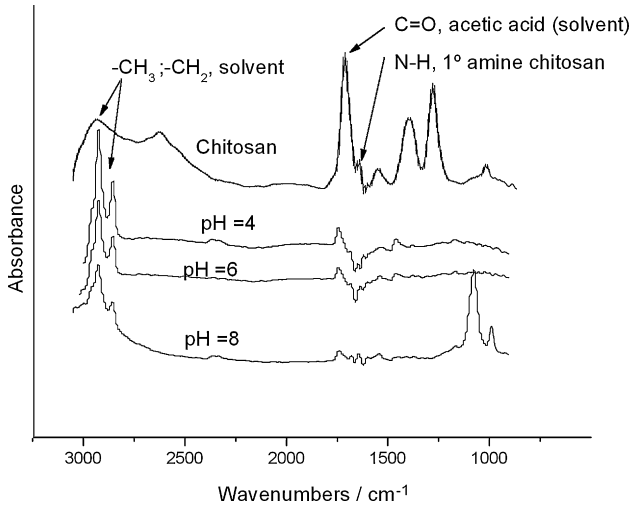

Fig. 2. ATR-FTIR spectrum of chitosan and elution samples. From the top: Chitosan acetic solution (reference), pH 4, 8 and 6 elutions.

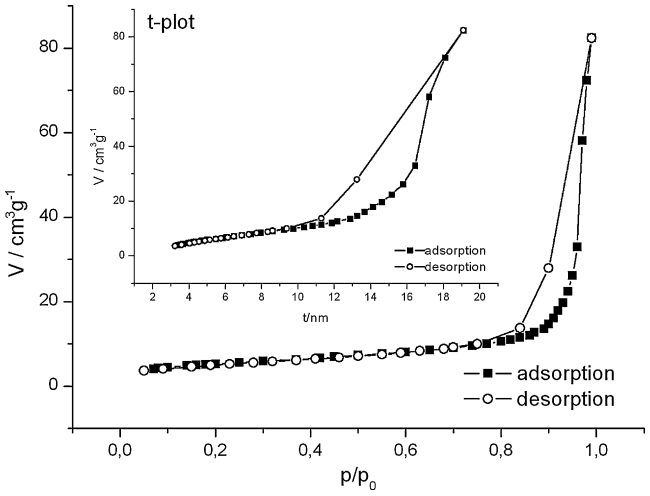

Fig. 4. The N_2 adsorption/desorption isotherms of the TiO_2-chitosan material. *Insert*: *t*-plot of chitosan-titania composed material.

to $-NH_2$ and –OH groups stretching vibrations at 3400 cm^{-1}) cannot be considered. For the chitosan identification only could be considered the N–H for primary amine band at 1600 cm^{-1}. It can be seen that this band it is not present at eluted collected samples, so we discarded the chitosan desorption from the porous sorbent due the pH media variation.

The FT-IR spectra of the TiO_2-chitosan material are shown in Fig. 3. Adsorptions at 3428 and 1627 cm^{-1} are attributed to $-NH_2$ and –OH groups stretching vibrations and N–H for primary amine in the chitosan structure. The prominent band with peak at ≈516 cm^{-1} corresponds to the TiO_2 lattice vibrations [25].

The titania crystalline phase plays an important role in the physical and chemical behavior of the material because all the specific surface area, the chemical stability and the chemical reactivity of the material are correlated with the particle size.

The XRD pattern of chitosan-titania composed materials (Fig. 3, *insert*) indicated that main peaks were ascribable to

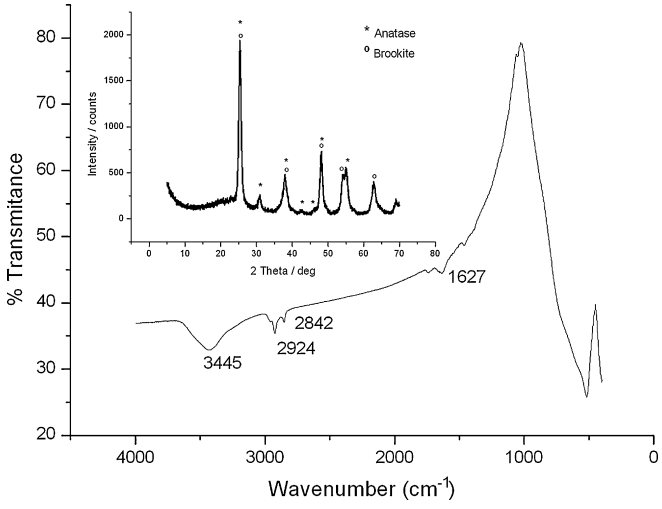

Fig. 3. FT-IR spectra of the TiO_2-chitosan material. *Insert*: XRD pattern of chitosan-titania composed material.

TiO_2 (anatase and brookite), no obvious peaks were observed regarding rutile, implying that the TiO_2 component in the porous substances was dominantly present as anatase. Some peaks that correspond to TiO, Ti_5O_9 and Ti_7O_{13} appeared too, but they were negligible.

The analysis of N_2 adsorption isotherms (Fig. 4) indicated that both systems (TiO_2 and TiO_2-chitosan) presented the typical Type II [26] isotherm. The *t*-plots (Fig. 4, insert) show the appearance of the materials having slit-shaped pores [27]. The total area (A_{ttot}), the exterior area (A_{text}), the pore surface area (estimated from the difference between A_{ttot} and A_{text}), the pore and the core volume (V_{tp}, V_c) were computed from the *t*-plot [26,27] and the results were summarized in Table 1. The TEM microphotographs obtained for the calcined porous TiO_2 and the non-calcined TiO_2-chitosan materials confirmed the existence of a lamellar structure with slit-shaped pores (Fig. 5A and B).

3.2. Dye adsorption

Three isotherms equations are tested in this work. One is the Langmuir equation, which has been widely applied to describe experimental adsorption data based on the assumption that the maximum adsorption corresponds to a saturated monolayer of adsorbate molecules on the adsorbent surface with constant energy and no transmigration of adsorbate in the plane of adsorbent surface [28].

$$q_e = \frac{q_{mon} K_L C_e}{1 + K_L C_e} \quad (1)$$

where K_L is the Langmuir constant related to the energy of adsorption and q_{mon} is the maximum amount of adsorption corresponding to complete coverage on the surface.

The equilibrium adsorption capacity, q_e (mmol/g), was calculated with the equation [29]:

$$q_e = \frac{(C_0 - C_e)V}{m} \quad (2)$$

Table 1
Analysis of adsorption results

Sample	A_{sp} (m^2/g)	A_{BET} (m^2/g)	A_{text} (m^2/g)	A_{BJHac} (m^2/g)	A_{BJHdc} (m^2/g)	D_{aap} (nm)	D_{aBJH} (nm)	D_{dBJH} (nm)	V_{spat} (cm^3/g)	$V_{BJHacvp}$ (cm^3/g)	$V_{BJHdcpv}$ (cm^3/g)
TiO_2	30.58	34.9	55.60	16.69	39.80	17.59	33.40	16.87	0.0153	0.0164	0.0168
TiO_2-chitosan	103.07	113.8	170.06	58.56	124.67	15.24	21.10	14.95	0.0433	0.0452	0.0461

Nitrogen adsorption data of the different samples. A_{sp}: single point surface area at $P/P_0 = 0.2002$, A_{BET}: BET surface area, A_{text}: *t*-plot external surface area, A_{BJHac}: BJH adsorption cumulative surface area of pores between 3.4 and 600 nm diameter, A_{BJHdc}: desorption cumulative surface area of pores between 3.4 and 600 nm diameter,. $2l_{molec}$: twice the length of the surfactant molecule, D_{aap}: adsorption average pore diameter by BET (8V/A), D_{aBJH}: BJH adsorption average pore diameter, D_{dBJH}: BJH desorption average pore diameter, V_{spat}: single point adsorption total pore volume of pores, $V_{BJHacvp}$: BJH adsorption cumulative volume of pores, $V_{BJHdcpv}$: desorption cumulative volume of pores.

where C_0 is the initial concentration (mmol/dm^{-3}), C_e the residual concentration at equilibrium (mmol/dm^{-3}), V the solution volume (dm^{-3}), and m is the adsorbent mass (mg).

The constants K_L and q_{mon} can be determined from the following form of Eq. (1),

$$\frac{1}{q_e} = \frac{1}{q_{mon}} + \frac{1}{K_L q_{mon}} \frac{1}{C_e}. \tag{3}$$

The Freundlich isotherm [30] is the earliest known relationship describing the sorption equation. This fairly satisfactory empirical isotherm can be used for non-ideal sorption that involves heterogeneous surfaces energy systems and is expressed by the equation.

$$q_e = K_F C_e^{1/n}, \tag{4}$$

where K_F is roughly an indicator of adsorption capacity and $1/n$ is the adsorption intensity. In general, as K_F increases the adsorption capacity of an adsorbent for a given adsorbate increases. The magnitude of the exponent $1/n$ gives an indication of the favorability of adsorption.

Eq. (4) may be linearized by taking logarithms:

$$\log q_e = \log K_F + \frac{1}{n} \log C_e \tag{5}$$

The third equation applied corresponds to Sips adsorption model; here, some of the features of the classical Langmuir and Freundlich models were incorporated [31,32].

$$q_e = \frac{q^m b C_e^{1/ns}}{1 + b C_e^{1/ns}} \tag{6}$$

where b (dm^3 $mmol^{-1}$)$^{1/ns}$ is a constant related to the adsorption energy, and $1/ns$ is the Sips parameter related to the adsorption intensity.

In order to determine the mechanism of dye adsorption and evaluate the temperature effect on the adsorption capacity, the experimental data (Figs. 6 and 7) were fitted to Langmuir, Freundlich and Sips equation; the obtained parameters are summarized in Table 2.

The obtained results showed that for both acid (BP) and basic (MB) dyes the adsorption on TiO_2-Chit A material was best predicted by Langmuir Isotherm. The Langmuir adsorption model assumes that the adsorbed layer is one molecule thick

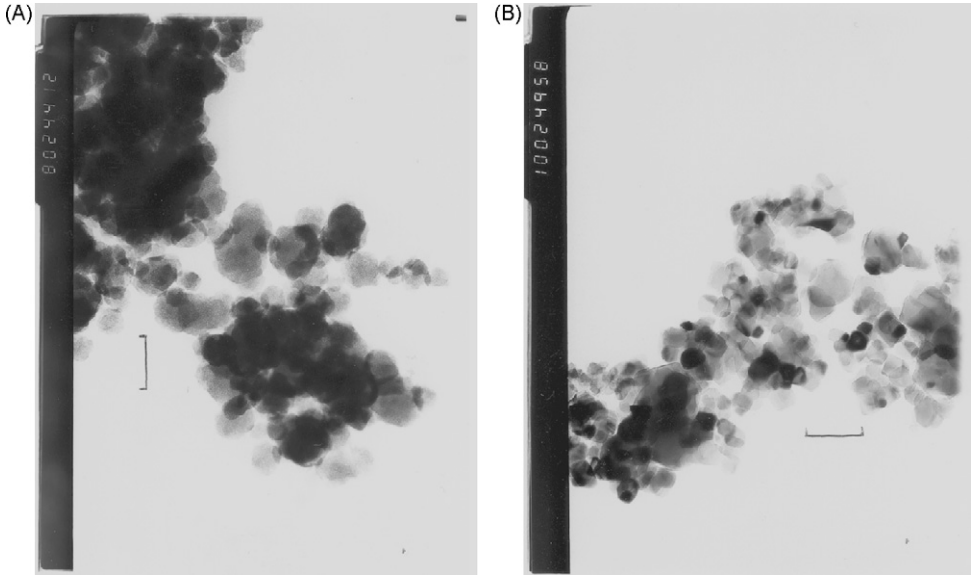

Fig. 5. Electron transmission micrograph of (A) TiO_2 material after calcination, small irregular lamellae superimposed and some granules (probably by Titania) may be seen (B) TiO_2-chitosan material without calcination, it may bee appreciated an irregular lamellae superimposed structure. The bar represents 106 and 85 nm, respectively.

Table 2
Parameters of the Langmuir, Freundlich and Sips isotherm applied to experimental data for the adsorption of MB and BP on TiO_2-Chit A and TiO_2-Chit B at different temperatures

T (°C)	MB + TiO_2-Chit A									
	Langmuir			Freundlich			Sips			
	q_{mon} (mmol g^{-1})	K_L (dm^3 mmol^{-1})	R^2	n	K_F	R^2	q_m (mmol g^{-1})	b (dm^3 mmol^{-1})$^{1/ns}$	$1/n_s$	R^2
25	0.0038 ± 0.0004	16.75 ± 0.08	0.992	1.17 ± 0.05	0.21 ± 0.05	0.990	0.003 ± 0.011	54.132 ± 3.125	1.16 ± 0.23	0.978
35	0.0019 ± 0.0001	28.91 ± 0.02	0.998	1.40 ± 0.10	0.14 ± 0.08	0.986	0.247 ± 0.012	0.128 ± 0.050	0.96 ± 0.15	0.962
45	0.0016 ± 0.0002	16.49 ± 0.03	0.997	0.81 ± 0.10	0.13 ± 0.08	0.986	0.055 ± 0.006	0.766 ± 0.023	1.09 ± 0.05	0.990
	MB + TiO_2-Chit B									
	Langmuir			Freundlich			Sips			
	q_{mon} (mmol g^{-1})	K_L (dm^3 mmol^{-1})	R^2	n	K_F	R^2	q_m (mmol g^{-1})	b (dm^3 mmol^{-1})$^{1/ns}$	$1/n_s$	R^2
25							1.590 ± 0.311	0.0116 ± 0.0012	0.88 ± 0.23	0.981
35							4.506 ± 0.512	0.0027 ± 0.0005	0.87 ± 0.15	0.910
45							192.03 ± 12.12	0.0007 ± 0.0002	0.97 ± 0.05	0.926
	BP + TiO_2-Chit A									
	Langmuir			Freundlich			Sips			
	q_{mon} (mmol g^{-1})	K_L (dm^3 mmol^{-1})	R^2	n	K_F	R^2	q_m (mmol g^{-1})	b (dm^3 mmol^{-1})$^{1/ns}$	$1/n_s$	R^2
25	0.0161 ± 0.0004	6.45 ± 0.08	0.998	1.27 ± 0.06	0.24 ± 0.05	0.997	0.013 ± 0.005	9.625 ± 3.125	1.06 ± 0.23	0.996
35	0.0183 ± 0.0001	5.27 ± 0.02	0.998	1.28 ± 0.11	0.24 ± 0.08	0.994	0.012 ± 0.005	16.396 ± 2.050	1.17 ± 0.16	0.992
45	0.0074 ± 0.0002	13.63 ± 0.03	0.997	1.37 ± 0.12	0.21 ± 0.08	0.994	0.005 ± 0.001	82.963 ± 10.233	1.35 ± 0.05	0.990
	BP + TiO_2-Chit B									
	Langmuir			Freundlich			Sips			
	q_{mon} (mmol g^{-1})	K_L (dm^3 mmol^{-1})	R^2	n	K_F	R^2	q_m (mmol g^{-1})	b (dm^3 mmol^{-1})$^{1/ns}$	$1/n_s$	R^2
25							0.0046 ± 0.011	6.257 ± 2.125	0.716 ± 0.33	0.973
35							0.0651 ± 0.012	0.024 ± 0.006	0.023 ± 0.13	0.966
45							0.277 ± 0.006	0.005 ± 0.003	0.112 ± 0.17	0.982

and the sites are homogeneous. The strength of the intermolecular attractive forces is believed to fall off rapidly with distance. Overall, the Langmuir isotherm has the highest coefficient of correlation for the adsorption of both dyes suggesting that the adsorption process was probably dominated by a monolayer formation rather than a multilayer. The formation of a monolayer (but not necessarily a compact one) may be assumed and the thermodynamic data obtained from the Langmuir equation are trustworthy.

The amino groups in the adsorbed chitosan layers were protonated and subsequently interacted with the sulfonyl group of the BP molecule to form the electrostatic organic complex $–NH_3^+ \ldots {}^-OOS–R$ as observed in adsorption of humic acid onto chitosan-coated granules [33] as well as in adsorption of dyes such as indigo carmine [34] and RR189 [35] onto chitosan.

On the other hand, for the basic dye adsorption on chitosan layers it was supposed to be by a kind of electrostatic attraction between the π-electronic cloud in the MB molecule and the adsorption sites ($–NH_3^+$) of chitosan. Nevertheless, it can be noticed that the BP adsorption is major than MB. This last fact is due to the repulsive interactions that are present between positive charge in the MB molecule and the ($–NH_3^+$) of chitosan during adsorption process.

In comparison with TiO_2 material without chitosan, the cationic polyelectrolyte presence augmented notably de BP and not decreased excessively the MB adsorption capacity.

The adsorption of both dyes on TiO_2-Chit B material, on contrary, was best predicted by the Sips equation. This means that adsorbent surface is not homogeneous and that the different adsorption sites at the surface are not energetically equivalent, which is in agreement with the presence of TiO_2 and $–NH_3^+$ groups in the adsorbent structure due to the TiO_2 incomplete cover with Chitosan.

3.3. Thermodynamic of adsorption

From adsorption isotherm data at different temperatures, the enthalpy (ΔH°_{ads}), entropy (ΔS°_{ads}) and free energy of adsorption (ΔG°_{ads}) can be calculated using the following equations:

$$\frac{\partial(\ln K_L)}{\partial(1/T)} = -\frac{\Delta H^\circ_{ads}}{R} \quad (7)$$

$$\Delta G^\circ_{ads} = -RT \ln K_L \quad (8)$$

$$\Delta G^\circ_{ads} = \Delta H^\circ_{ads} + T\,\Delta S^\circ_{ads} \quad (9)$$

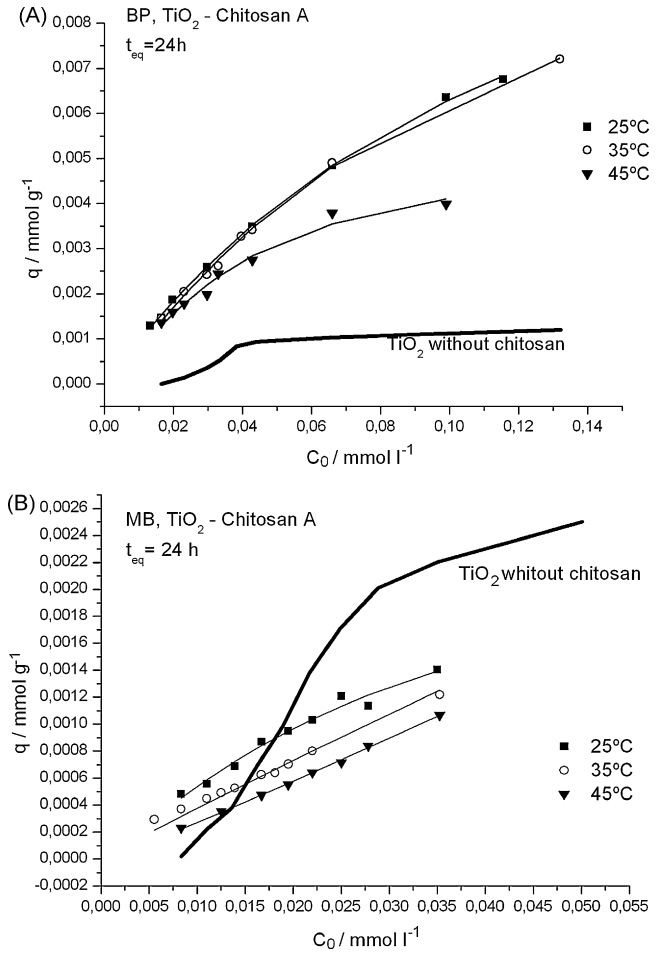

Fig. 6. Adsorption isotherms on TiO_2-Chit A material of (A) BP and (B) MB. Continuous line represents the adsorption isotherm of the same dyes on TiO_2 without chitosan.

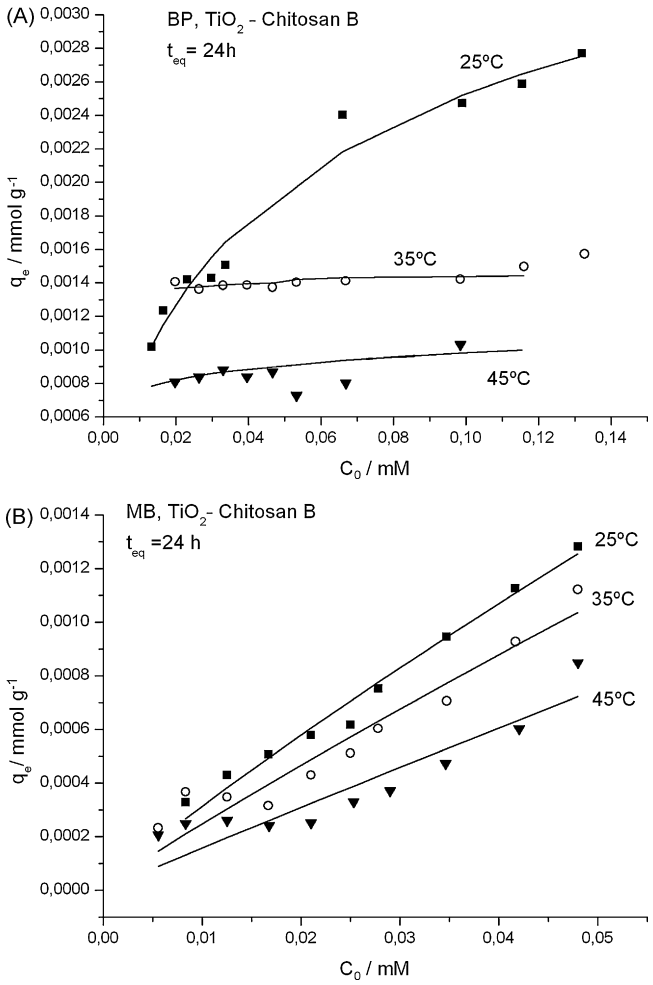

Fig. 7. Adsorption isotherms on TiO_2-Chit B material of (A) BP and (B) MB.

where K_L is the Langmuir adsorption equilibrium constant, T the solution absolute temperature and R is the gas constant.

The enthalpies of the dye-TiO_2 chitosan adsorption are found from the van't Hoff plots: $\ln K_L$ versus $1/T$ (Fig. 8). The use of the van't Hoff plots is an indirect, but accurate method to calculate thermodynamic adsorption parameters at solid–solution interfaces. However, difficulties arise from the assumption that ΔH°_{ads} does not change with the temperature, which is often not the case.

Taking into account the curvature of the obtained van't Hoff plot (Fig. 8) a second order polynomial regression analysis of the plots was used. The $\Delta H^\circ_{ads}/R$ values were found from derivation of individual regression functions.

The dependence of ΔH°_{ads} is due to a change in the adsorption heat capacity ($\Delta_{ads}C_p$), which was calculated in a simple manner as follows [36]:

$$\Delta_{ads}C_p = \frac{(\Delta H^\circ_{ads}(T_2) - \Delta H^\circ_{ads}(T_1))}{T_2 - T_1}, \quad \text{where } T_2 > T_1 \quad (10)$$

Thermodynamic parameters were summarized in Table 3.

The negative adsorption values of ΔG°_{ads} for both dyes indicated that the adsorption on TiO_2-Chit A is a spontaneous process. The values of ΔS°_{ads} and ΔH°_{ads} suggest that both enthalpy and entropy are responsible for making the $\Delta G^\circ_{ads} < 0$.

For MB adsorption, the ΔS°_{ads} and ΔH°_{ads} values augment with the increment of temperature. Adsorption goes from an exothermic to an endothermic process, so it was enthalpically

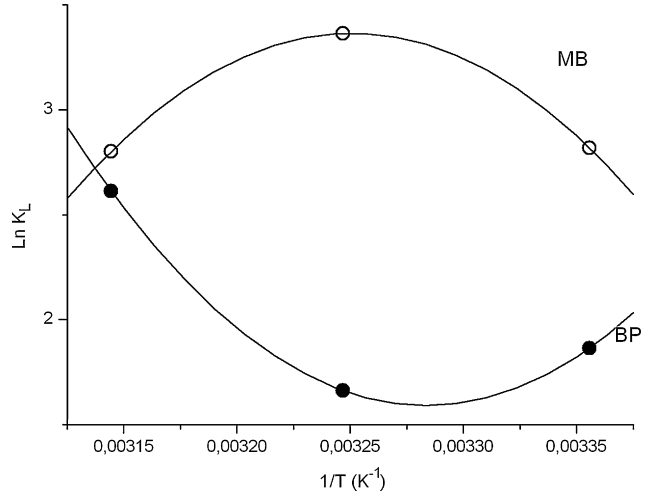

Fig. 8. $\ln K_L$ vs. $1/T$ plot for MB and BP adsorption TiO_2-Chit A.

Table 3
Thermodynamic parameters of dye adsorption on TiO_2-Chit A material

T (°C)	BP + TiO_2-Chit A			
	ΔH°_{ads} (kJ mol^{-1})	ΔG°_{ads} (kJ mol^{-1})	ΔS°_{ads} (kJ mol^{-1} K^{-1})	$\Delta_{ads}C_p$ (kJ mol^{-1} K^{-1})
25	128.879	−4.637	0.4465	−303.817
35	35.289	−4.260	0.1284	
45	−69.998	−6.911	−0.1984	
	MB + TiO_2-Chit A			
	ΔH°_{ads} (kJ mol^{-1})	ΔG°_{ads} (kJ mol^{-1})	ΔS°_{ads} (kJ mol^{-1} K^{-1})	$\Delta_{ads}C_p$ (kJ mol^{-1} K^{-1})
25	−94.306	−7.0098	−0.2919	−303.2008
35	−6.119	−8.619	0.00811	
45	93.090	−7.414	0.3160	

disfavored with the augment of T. At the same time an augment of ΔS°_{ads} indicated a randomness augment at the solid–solution interface confirming a diminution of the adsorption capacity. For BP adsorption, on contrary, there was a decrease of ΔS°_{ads} and ΔH°_{ads} values with the augment of T. The process is enthalpically favored and $\Delta G^\circ_{ads} < 0$. However, experimental results show that adsorption capacity diminished with the increment of T. This fact would be possible due to a chitosan desorption from TiO_2 surface. With temperature growth there is an increase of energy of adsorbed polyelectrolyte which possible allows some of their moieties to leave adsorbent active centers. As a result, the amount of adsorbed dye decreases.

From inspection of Table 3, the signs of $\Delta_{ads}C_p$ values are negative for both dye adsorptions. In general negative (often large) values of $\Delta_{ads}C_p$ coupled with favorable positive entropy changes, have been used as an indicator of intense hydrophobic interactions [37].

3.4. Adsorption kinetic

Figs. 9 and 10 show the dependence with time of MB and BP adsorbed amounts on the TiO_2-chitosan material. It can be seen that the adsorption equilibrium were observed after 400 and 200 min for both dyes, without difference on TiO_2-Chit A and TiO_2-Chit B, respectively, irrespective on the nature of the dye and the adsorbent. The kinetic adsorption data were processed to understand the dynamic of adsorption process in terms of the order, n, and of the rate constant, k [37].

Traditionally, the adsorption kinetics is described following the expressions originally given by Lagergren, which are special cases for the general Langmuir rate equation [38]. A simple kinetic analysis of adsorption is the pseudo-first order equation in the form:

$$\frac{dq_t}{dt} = k_{1,s}(q_e - q_t) \tag{11}$$

where $k_{1,s}$ is the pseudo-first-order rate constant and q_e denote de amount of adsorption at equilibrium. Integrating Eq. (11) for the boundary conditions $t = 0$ to t and $q_t = 0$ to q_t gives:

$$\ln(q_e - q_t) = \ln(q_e) - k_{1,s}t \tag{12}$$

In addition, a pseudo-second-order equation based on adsorption equilibrium capacity may be expressed in the form:

$$\frac{dq_t}{dt} = k_{2,s}(q_e - q_t)^2 \tag{13}$$

where $k_{2,s}$ is the pseudo-second-order rate constant.

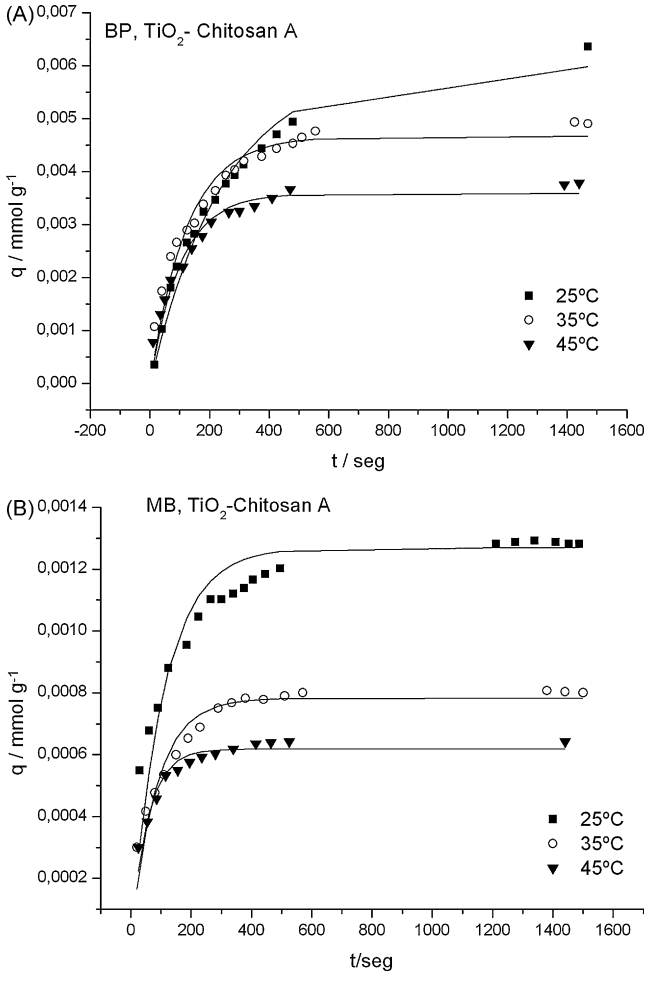

Fig. 9. (A) BP and (B) MB adsorbed amounts time dependence on the TiO_2-Chit A material.

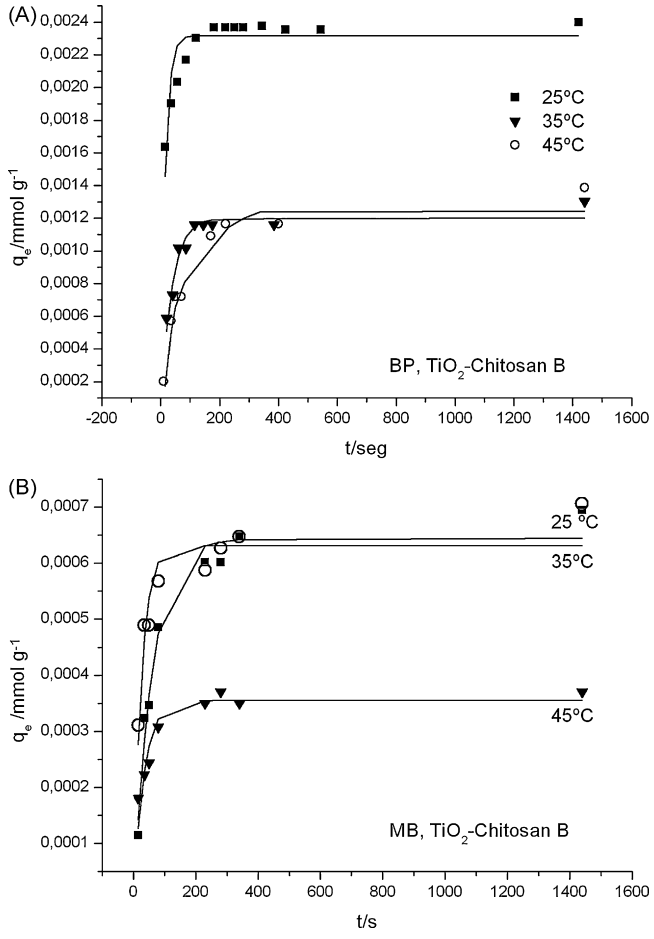

Fig. 10. (A) BP and (B) MB adsorbed amounts time dependence on the TiO_2-Chit B material.

By integrating, applying the initial conditions and rearranged to obtain a linear form we have:

$$\frac{t}{q_t} = \frac{1}{k_{2,s}q_e^2} + \frac{1}{q_e}t \tag{14}$$

The fitting validity of these models is traditionally checked by the linear plots of $\ln(q_e - q_t)$ versus t and t/q_t versus t, respectively. The slope and intercept of the obtained straight line provide the respective kinetic constant and the q_e parameters.

Despite the Lagergren kinetic equations has been used for the most adsorption kinetic works, determination of some specific kinetic parameters, as possible changes of the adsorption rates in function of the contact time and temperature represent still lacks and a change in the kinetic adsorption model.

Experimental data were further treated with both the above-mentioned models; the obtained results (not shown) indicated that those models do not agree with experimental values. In this way, an alternative kinetic equation was used, Avrami kinetic equation:

$$q_t = q_e(1 - \exp^{-[k_{av}t]^n}) \tag{15}$$

where k_{av} is the Avrami kinetic rate constant and n is the reaction order.

In order to quantitatively compare the applicability of the applied kinetic model, the normalized standard deviation (Δq_t) were calculated as follows [39]:

$$\Delta q_t(\%) = 100 \times \sqrt{\frac{\sum[(q_{t,exp} - q_{t,calc})/q_{t,exp}]^2}{(a-1)}} \tag{16}$$

where $q_{t,calc}$ are the adsorption capacity calculated values from both the Lagergren and the Avrami models and a is the number of experimental points of the kinetic curve. The obtained kinetic parameters are summarized in Table 4. From inspection of this table, it can be seen that the order (n) and the Avrami kinetic rate constant (k_{av}) augment with the increment of T for both dye adsorption on TiO_2-Chit A. This fact agrees with the existence of different process controlling the adsorption rate. For MB adsorption on TiO_2-Chit B, n and k_{av} were not affected by a change of T, while for BP adsorption on the same material such parameters diminished.

The Lagergren and the Avrami kinetic models cannot give interaction mechanisms, so another model to test dye diffusion into the TiO_2-Chit hybrid material was also used. A pore diffusion model, described by Eq. (17), was used here and in most solid/solution interaction studies [40].

$$q_t = k_{diff}t^{1/2} + I \tag{17}$$

where k_{diff} is the pore diffusion rate constant and I is the intercept. On the other hand, if the intra particle diffusion is involved in the adsorption process, then a plot of $q \times t$ versus $t^{1/2}$ would result

Table 4
Kinetic adsorption parameters obtained using Avrami equation

T (°C)	MB + TiO_2-Chit A					MB + TiO_2-Chit B				
	q_{mon} (mmol g^{-1})	k_{av} (min^{-1})	n	R^2	Δq_t (%)	q_{mon} (mmol g^{-1})	k_{av} (min^{-1})	n	R^2	Δq_t (%)
25	0.0060 ± 0.004	0.0040 ± 0.0006	0.99 ± 0.14	0.988	3.93	0.00064 ± 0.0003	0.0858 ± 0.0216	0.364 ± 0.2	0.973	1.02
35	0.0046 ± 0.002	0.0057 ± 0.0002	1.42 ± 0.23	0.989	4.02	0.00063 ± 0.0002	0.0853 ± 0.0132	0.451 ± 0.1	0.976	0.701
45	0.0036 ± 0.001	0.0063 ± 0.0012	1.56 ± 0.62	0.988	1.085	0.00036 ± 0.0001	0.0736 ± 0.0052	0.399 ± 0.3	0.982	2.835
	BP + TiO_2-Chit A					BP + TiO_2-Chit B				
	q_{mon} (mmol g^{-1})	k_{av} (min^{-1})	N	R^2	Δq_t (%)	q_{mon} (mmol g^{-1})	k_{av} (min^{-1})	n	R^2	Δq_t (%)
25	0.0013 ± 0.0004	0.0060 ± 0.0004	1.52 ± 0.43	0.985	0.340	0.0023 ± 0.00013	0.1098 ± 0.0346	0.601 ± 0.15	0.986	1.232
35	0.0008 ± 0.0002	0.0069 ± 0.0032	1.72 ± 0.31	0.986	1.259	0.0012 ± 0.00002	0.0708 ± 0.0162	0.388 ± 0.09	0.986	0.708
45	0.0006 ± 0.0001	0.0085 ± 0.0032	2.12 ± 0.62	0.982	0.594	0.00124 ± 0.0001	0.0523 ± 0.0212	0.286 ± 0.13	0.985	1.356

Table 5
Kinetic adsorption parameters obtained using pore and intra particle diffusion models

T (°C)	Pore diffusion $q_t = k_{diff}\, t^{1/2} + I$				Intra particle diffusion $q_t\ t = k_{diff} t^{1/2} + I$			
	K_{diff} (mmol g^{-1} min$^{-1/2}$)	I (mmol g^{-1})	$t^{1/2}$ (min$^{-1/2}$)	R^2	K_{diff} (mmol g^{-1} min$^{1/2}$)	I (mmol g^{-1}min)	$t^{1/2}$ (min$^{-1/2}$)	R^2
BP + TiO_2-Chit A								
25	$(2.513 \pm 0.031) \times 10^{-4}$	$(-3.43 \pm 0.03) \times 10^{-4}$	(0–21.910)	0.993	0.425 ± 0.031	−6.93 ± 0.63	(21.91–37.73)	0.999
35	$(2.189 \pm 0.056) \times 10^{-4}$	$(4.05 \pm 0.08) \times 10^{-4}$	(0–17.791)	0.994	0.296 ± 0.063	−4.19 ± 0.09	(17.79–37.73)	0.998
45	$(2.008 \pm 0.011) \times 10^{-4}$	$(1.58 \pm 0.06) \times 10^{-3}$	(0–14.373)	0.997	0.212 ± 0.021	−2.67 ± 0.012	(14.37–37.73)	0.997
MB + TiO_2-Chit A								
25	$(5.087 \pm 0.051) \times 10^{-5}$	$(2.78 \pm 0.33) \times 10^{-4}$	(0–16.43)	0.997	0.078 ± 0.021	-1.11 ± 0.86	(16.43–37.73)	0.999
35	$(3.540 \pm 0.048) \times 10^{-5}$	$(1.57 \pm 0.25) \times 10^{-4}$	(0–16.43)	0.998	0.046 ± 0.013	-0.61 ± 0.09	(16.43–37.73)	0.998
45	$(4.030 \pm 0.081) \times 10^{-5}$	$(9.19 \pm 0.06) \times 10^{-5}$	(0–10.86)	0.997	0.034 ± 0.001	−0.41 ± 0.01	(10.86–37.73)	0.992
BP + TiO_2-Chit B								
25	$(9.20 \pm 0.32) \times 10^{-5}$	$(1.32 \pm 0.53) \times 10^{-3}$	(0–10.94)	0.990	0.045 ± 0.005	−0.562 ± 0.063	(10.94–37.73)	0.997
35	$(8.57 \pm 0.86) \times 10^{-5}$	$(1.73 \pm 0.25) \times 10^{-5}$	(0–12.89)	0.970	0.074 ± 0.003	−0.874 ± 0.190	(12.89–37.73)	0.992
45	$(9.31 \pm 1.12) \times 10^{-5}$	$(1.85 \pm 0.65) \times 10^{-4}$	(0–10.72)	0.964	0.065 ± 0.001	−0.655 ± 0.112	(10.72–37.73)	0.989
MB + TiO_2-Chit B								
25	$(7.07 \pm 1.123) \times 10^{-5}$	$(-1.38 \pm 0.33) \times 10^{-4}$	(0–8.94)	0.991	0.039 ± 0.011	−0.473 ± 0.86	(8.94–37.73)	0.998
35	$(4.54 \pm 0.23) \times 10^{-5}$	$(1.51 \pm 0.26) \times 10^{-4}$	(0–8.94)	0.996	0.039 ± 0.013	−0.484 ± 0.12	(8.94–37.73)	0.999
45	$(2.46 \pm 0.181) \times 10^{-5}$	$(7.98 \pm 0.07) \times 10^{-5}$	(0–8.94)	0.988	0.020 ± 0.001	−0.239 ± 0.131	(8.94–37.73)	0.998

in a linear relationship, and the particle diffusion would be the controlling step if this line passed through the origin. Obtained results are exposed in Table 5.

Figs. 11 and 12 show the pore and intra particle diffusion plots for BP and MB adsorption on TiO_2-Chit A material. It can be seen that all adsorption process posses a diffusion (pore followed by intra particle diffusion) rate control. Similar results were obtained for dye adsorption on TiO_2-Chit B material.

For BP and MB adsorption on TiO_2-Chit A, the pore diffusion remained for a major time that intra particle diffusion control. The interval where pore diffusion control existed decreased with the increment of temperature leading to an augment of the intra particle diffusion control.

In contrast when dyes adsorbed on TiO_2-Chit B material, the intra particle diffusion prevailed over pore diffusion control. In these cases there was not an appreciable temperature effect on such processes.

When the plots do not pas through the origin, as in our case, is indicative of some degree of boundary layer control and this shows further that the intra particle diffusion is not only rate-controlling step, but other processes may also occurs at the same time, all of which may be operating at the same time. The values of the intercept give an idea about the boundary layer thickness: the larger the intercept, the greater the boundary layer effect. The boundary layer resistance is affected by the rate of adsorption and increase in contact time, which reduces the resistance and increase the mobility of dye during adsorption.

Intra particle diffusion is also usually controlled by the dimensions of the particle pores. The grater the particle pore sizes, the smaller the contribution of the intra particle diffusion resistance in the control of the sorption kinetic. So, the increase

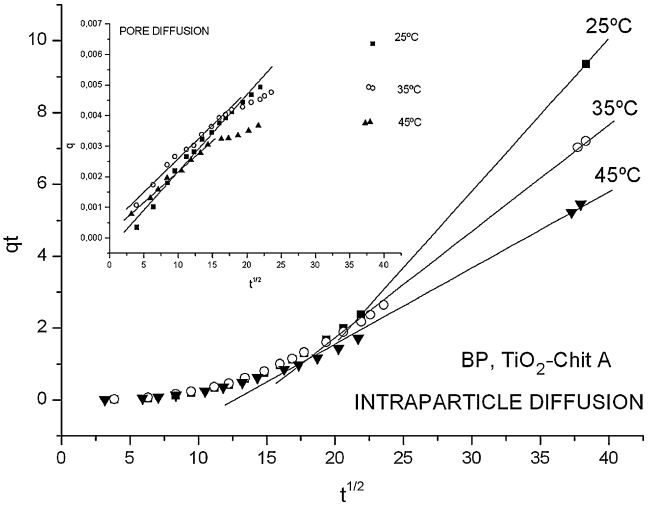

Fig. 11. Pore (*insert*) and intra particle diffusion plots for BP adsorption on TiO_2-Chit A material.

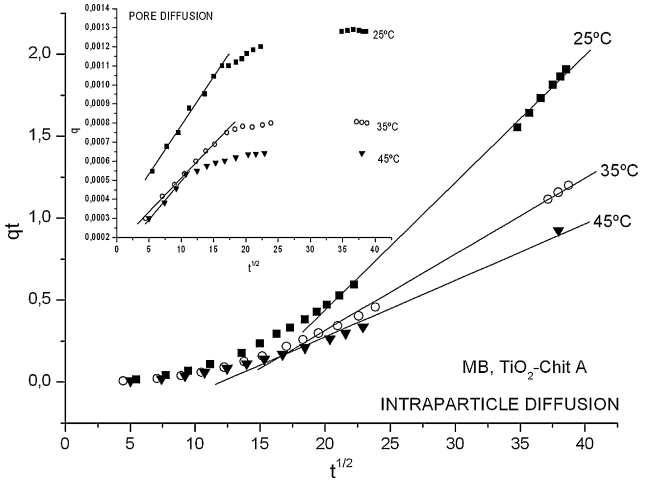

Fig. 12. Pore (*insert*) and intra particle diffusion plots for MB adsorption on TiO_2-Chit A material.

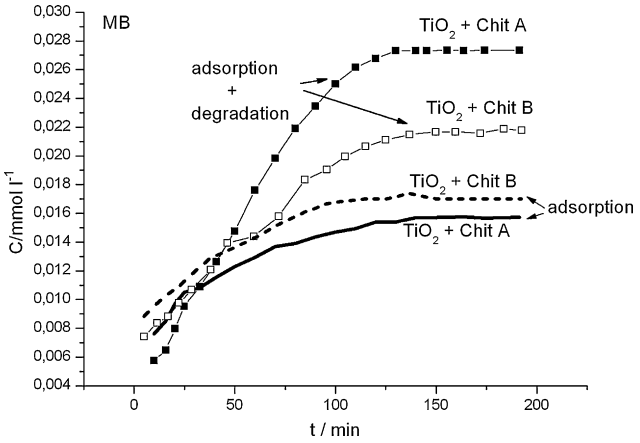

Fig. 13. Photodegradation of MB on both TiO_2-chitosan hybrid materials. *C* is the amount of MB removed expressed in mmol/dm^{-3}.

of the chitosan pores with the increase of temperature [41] seems to decrease the effect of the boundary layer effect. For BP adsorption on TiO_2-Chit B where the content of chitosan is minor than in TiO_2-Chit A the boundary layer resistance is not decreased with the increase of chitosan pores, so non-temperature effect was appreciated.

3.5. Photodegradation properties

Fig. 13 shows photodegradation of MB on both TiO_2-chitosan hybrid materials. The photodegradation is about of 91% (TiO_2-chitosan A) and 41% (TiO_2-chitosan B) and augmented with the chitosan adsorbent content. For acid dye BP (Fig. 14) it can be seen that the process in darkness resulted in a high remotion capacity than in UV light presence. Similar results were obtained for the adsorption in both porous materials. These facts are related with the effect of UV light on chitosan layers. The action of ionizing radiation on chitosan resulted in the polymer chain scission, accompanied by the induction of carboxyl groups in the residue [42–44]. Even though irradiation induced chain scission, the chemical structure of chitosan (including the degree

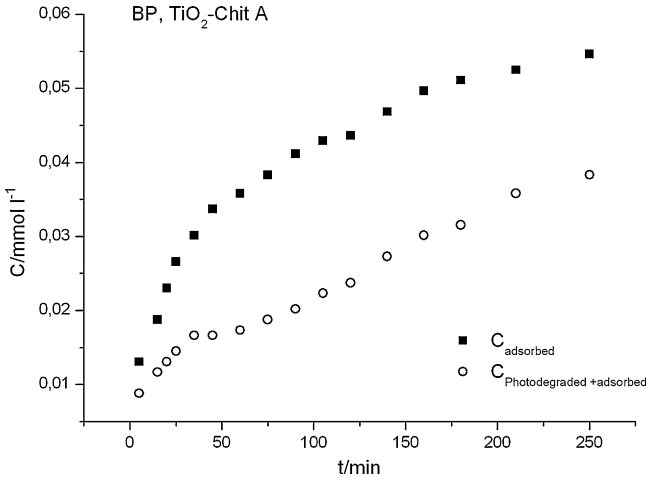

Fig. 14. Adsorption of BP on TiO_2-Chit A material in presence and in absence of UV light.

of acetylation) did not change significantly [45]. The generation of negative carboxyl groups attracted MB molecules, so adsorption of basic dye in UV-light presence is notably augmented. The same effect decreased the acid dye adsorption.

4. Summary

The remotion of a basic, methylene blue (MB), and an acid, benzopurpurin (BP), dyes from aqueous solution onto TiO_2-chitosan hybrid material was studied in this work.

The variation of adsorption capacity (q_e) indicated a great dependence of the adsorption mechanism on the adsorbent structure, the dyes' molecular configuration, chitosan content and the temperature conditions.

In general, for all systems (dye + adsorbent), there was a diminution of q_e with the augment of *T* and with the diminution of the material chitosan content. It was clear that the adsorption of BP was higher than that of MB. This fact is due to repulsive interaction between positive charges in MB molecules and the ($-NH_3^+$) of chitosan during adsorption process. Nevertheless, even if these repulsive interactions existed the adsorption of MB is considerable and chitosan amount dependent and would be possible due attractive interaction between π-electron cloud on the dye molecule and the cationic chitosan groups. In comparison with TiO_2 material without chitosan, the presence of the cationic polyelectrolyte augmented notably de BP and not excessively decreased the MB adsorption capacity.

To determine the mechanism of dye adsorption and evaluate the effect of temperature on adsorption capacity, the experimental data were treated with Langmuir, Freundlich and Sips isotherm equations. The analysis of the obtained parameters and correlation coefficient showed that the adsorption of both dyes on TiO_2-Chit A material at the three work temperatures was best fitted by the employment of the Langmuir model, while Sips equation adjusted better to adsorption data on TiO_2-Chit B material.

The change of temperature affected dye adsorption. The analysis of thermodynamic parameters suggested that the adsorption is mainly chemical because of the high adsorption enthalpy values. There is a change in the adsorption heat capacity ($\Delta_{ads}C_p < 0$) related with intense hydrophobic interactions.

The kinetics of adsorption was also studied and the results followed Avrami kinetic model. The variation of the reaction order, *n*, and k_{av} with *T* suggested different interactions mechanism during adsorption process. From the analysis of the obtained data such mechanism would be assumed related to a pore followed by intra particle diffusion control of the adsorption rate.

Finally the material photodegradation properties were evaluated. MB photodegradation on both TiO_2-chitosan hybrid materials was of 91% (TiO_2-chitosan A) and 41% (TiO_2-chitosan B) and augmented with chitosan content. For BP it was noticed that the process in darkness resulted in a high remotion capacity than in UV-light presence. These last facts are related with the induction of $-COO^-$ groups on chitosan layers due to the effect of ionizing radiation. The generation of $-COO^-$ attracted the positive MB and rejected the negative BP molecules.

Consequently, from the analysis of the experimental obtained data summarized in this work, we are able to say that TiO_2-chitosan materials are efficient for the simultaneous remotion of basic and acid dyes. The adsorption capacity of negative dyes in such materials are superior to that in others adsorbents like pure TiO_2 or SiO_2 without decreasing too much the adsorption capacity for positive dyes. Moreover, such efficiency augments with the chitosan content. On the other hand the application of UV-light increased the adsorption of basic dyes, by the generation of $–COO^-$ groups on the adsorbent and subsequent degradation of both dyes due to the existence of TiO_2.

Acknowledgements

This work was financed by grant of the Universidad Nacional del Sur and the Agencia Nacional de Promoción Científica y Tecnológica (ANPCyT) by the grant BID 1728 OC-AR PICT N° 10-14560. The authors want to thank to Dr. Liliana Albertengo (Laboratorio de Investigación Básica y Aplicada en Quitina (LIBAQ) of Universidad Nacional del Sur, Bahía Blanca, Argentina.) for kindly supplying the studied Chitosan, and to Dr. Marcelo Avena (Departamento de Química, Universidad Nacional del Sur, 8000 Bahía Blanca, Argentina) for his collaboration. CEZ and CL have a fellowship of the Concejo Nacional de Investigaciones Científicas y Técnicas de la República Argentina (CONICET). PM is an assistant researcher of CONICET.

References

[1] N. Koprivanac, A.L. Bozic, S. Papic, Cleaner production processes in the synthesis of blue anthraquinone reactive dyes, Dyes Pigments 44 (1) (1999) 33–40.
[2] S. Netpradit, P. Thiravetyan, S. Towprayoon, Evaluation of metal hydroxide sludge for reactive dye adsorption in a fixed-bed column system, Water Res. 38 (2004) 71–78.
[3] M.S. Reisch, Asian textile dye makers are a growing power in changing market, Chem. Eng. News 74 (3) (1996) 10–12.
[4] S.J. Allen, P. Brown, G. Mc Kay, O. Flynn, An evaluation of single resistance transfer models in the sorption of metal ions by peat, J. Chem. Technol. Biotechnol. 54 (1992) 271–276.
[5] S.J. Allen, L. Whitten, M. Murray, O. Duggan, The adsorption of pollutants by peat, lignite and activated chars, J. Chem. Technol. Biotechnol. 68 (1997) 442–452.
[6] S. Karcher, A. Kornmuller, M. Jekel, Screening of commercial. sorbents for the removal of reactive dyes, Dyes Pigments 51 (2001) 111–125.
[7] D.W. Bahnemann, Ultrasmall metal oxide particles: Preparation, photophysical characterization, and photocatalytic properties, Israel J. Chem. 33 (1993) 111–136.
[8] M.R. Hoffmann, S.T. Martin, W. Choi, D.W. Bahnemann, Environmental applications of semiconductor photocatalysis, Chem. Rev. 95 (1995) 69–96.
[9] S. Watson, J. Scott, D. Beydoun, R. Amal, Studies on the preparation of magnetic photocatalysts, J. Nanopart. Res. 7 (6) (2005) 691–705.
[10] J.D. Tores, E.A. Faria, J.R. SouzaDe, A.G.S. Prado, Preparation of photoactive chitosan-niobium (V) oxide composites for dye degradation, J. Photochem. Potobiol. A: Chem. 182 (2006) 202–206.
[11] M.N.V. Ravi Kumar, A review of chitin and chitosan applications, React. Funct. Polym. 46 (2000) 1–27.
[12] V. Coma, A. Martial-Gros, S. Garreau, A. Copinet, F. Sahin, A. Deschamps, Edible antimicrobial films based on chitosan matrix, J. Food Sci. 67 (2002) 1162–1168.
[13] P.A. Felse, T. Panda, Studies on application of chitin and its derivatives, Bioprocess Eng. 20 (1999) 505–512.
[14] W.M. Xie, P.X. Xu, W. Wang, Q. Liu, Preparation and antibacterical activity of water-soluble chitosan derivative, Carbohydr. Polym. 50 (2002) 35–40.
[15] E. Guibal, Interactions of metal ions with chitosan-based sorbents: a review, Sep. Purif. Technol. 38 (2004) 43–74.
[16] M.Y. Chang, R.S. Juang, Adsorption of tannic acid, humic accid, and dyes from water using the composite of chitosan and activated clay, J. Colloid Interface Sci. 278 (2004) 18.
[17] Y.C. Wang, Y.S. Szeto, W.H. Cheung, G. Mc Kay, Equilibrium studies for acid dye adsorption onto chitosan, Langmuir 19 (2003) 7888.
[18] Y.L. Liu, Y.H. Su, J.Y. Lai, In situ croos linking of chitosan and formation of chitosan-silica hybrid membranes with using Y-glycidoxypropyttrimethoxysilane as a crosslinking agent, Polymer 45 (2004) 6831.
[19] C.T. Kresge, M.E. Leonowicz, W.J. Roth, J.C. Vartulli, J.S. Beck, Ordered mesoporous molecular sieves synthesized by a liquid-crystal template mechanism, Nature 359 (1992) 710–712.
[20] V. Pedroni, M.E. Gschaider, P.C. Schulz, UV-spectrophotometry: improvements in the study of the degree of acetylation of chitosan, Macromol. Biosci. 3 (2003) 531–534.
[21] V. Pedroni, N. Andreucetti, M.E. Gschaider, P.C. Schulz, Chitosan structure in aqueous solution, Colloid Polym. Sci. 282 (2003) 100–102.
[22] C.G. Hatchard, C.A. Parker, Proc. R. Soc. Lond. A 235 (1956) 518.
[23] H. Butt, K. Graf, M. Kappl, Physics and Chemistry of Interfaces, Wiley-VCH Gmblt & Co., KGaA, 2004, pp. 5 (chapter 9).
[24] D. Meyer, Surfaces, Interfaces and Colloids, second ed., John Wiley & sons, 2002, pp. 25 (chapter 9).
[25] V.C. Farmer, in: Farmer (Ed.), The Infrared Spectra of Minerals, V.C. Mineral Society, London, 1974.
[26] F. Radjy, E.J. Sellevold, A phenomenological theory for the t-method of pore structure analysis: I. Slit-shaped pores, J. Colloid Interface Sci. 39 (2) (1972) 367–378.
[27] E.J. Sellevold, F. Radjy, A phenomenological theory for the t-method of pore structure analysis. II. Circularly cylindrical pores, J. Colloid Interface Sci. 39 (2) (1972) 379–388.
[28] I. Langmuir, The constitution and fundamental properties of solids and liquids. Part i. Solids, J. Am. Chem. Soc. 38 (11) (1916) 2221–2295.
[29] T.P. Saha, S. Karmaker, H. Ichikawa, Y. Fukumori, Mechanisms and kinetics of trisodium 2-hydroxy-1,1′azonaphtalene-3,4′,6-trisulfonate adsorption onto chitosan, J. Colloid Interface Sci. 286 (2005) 433–439.
[30] H. Freundlich, Uber die adsorption in Losungen, Z. Phys. Chem. 57 (1906) 385–470.
[31] Y.-S. Ho, A.E. Ofonaja, Biosorption thermodynamics of cadmium on coconut copra meal as biosorbent, Biochem. Eng. J. 30 (2006) 117–123.
[32] M.F. Sawalha, J.R. Peralta-Videa, J. Romero-González, J.L. Gardea-Torresdey, Biosorption of Cd(II), Cr(III), and Cr(VI) by saltbush (A triplex canescens) biomass: thermodynamic and isotherm studies, J. Colloid Interface Sci. 300 (2006) 100–104.
[33] X. Zhang, R. Bari, Mechanisms and kinetics of humic acid adsorption onto chitosan-coated granules, J. Colloid Interface Sci. 264 (2003) 30–38.
[34] F.C.S. dos Anjos, E.F.S. Vieira, A.R. Cestari, Interaction of indigo carmine dye with chitosan evaluated by adsorption and thermochemical data, J. Colloid Interface Sci. 253 (2002) 243–246.
[35] M.S. Chiou, H.Y. Li, Adsorption behavior of reactive dye. in aqueous solution on chemical cross-linked chitosan beads, Chemosphere 50 (2003) 1095–1105.
[36] G.A. Holdgate, W.H.J. Ward, Measurement of binding thermodynamics in drug discovery, Drug Discovery Today 10 (2005) 1543–1550.
[37] R. Qadeer, Adsorption of ruthenium ions on activated charcoal: influence of temperature on the kinetics of the adsorption process, J. Zhejiang Univ. Sci. B 6 (5) (2005) 353–356.
[38] Y.S. Ho, G. Mc Kay, Sorption of dyes and copper ions onto biosorbents, Process Biochem. 38 (2003) 1047–1061.
[39] F.C. Wu, R.L. Tseng, R.S. Juang, Preparation of highly microporous carbons from firwood by KOH activation for adsorption of dyes and phenols from water, Sep. Purif. Technol. 47 (2005) 10–19.

[40] M. Özacar, I.A. Sengil, Application of kinetic models to the sorption of disperse dyes onto alunite, Colloids Surf. A: Physicochem. Eng. Aspects 242 (2004) 105–113.
[41] M. Szekeres, J. Coth, I. Dekany, Specific surface area of stoeber silica determined by various experimental methods, Langmuir 18 (7) (2002) 2678–2685.
[42] O. Horváth, E. Bodnár, J. Hegyi, Photoassisted oxidative degradation of surfactants and simultaneous reduction of metals in titanium dioxide dispersions, Colloid Surf. A: Physicochem. Eng. Aspects 265 (2005) 135–140.
[43] S. Trzcinski, Combined Degradation of Chitosans, Polish Chitin Society, 2006, pp. 103–111 (Monograph XI).
[44] A.L. Andrade, A. Torikai, T. Kobatake, Spectral sensitivity of chitosan photodegradation, J. Appl. Polym. Sci. 62 (1996) 1465–1471.
[45] M.R. Kasaai, J. Arul, S.L. Chin, G. Charlet, The use of intense femtosecond laser pulses for the fragmentation of chitosan, J. Photochem. Photobiol. A: Chem. 120 (1999) 201–205.